Electronic Supplementary Information

A Trifecta of g-C_3N_4: Enhanced Visible-Spectrum Absorption, Increased Structure Distortion and Boosted Electronic Transfer Dynamics

Huanhuan Liu, ‡ [a] Haifei Wang, ‡ [a] Fu Zhang,[a] Jierui Xue,[a] Jihua Zhang*[b] and Genqiang Zhang*[a]

[a]Hefei National Laboratory for Physical Sciences at the Microscale, CAS Key Laboratory of Materials for Energy Conversion, Department of Materials Science and Engineering, University of Science and Technology of China Hefei, Anhui 230026, China.

[b]Guizhou Provincial Key Laboratory of Computational Nano-Material Science, Guizhou Education University, Guiyang, Guizhou 550018, China.

* Corresponding Author

E-mail address: gqzhangmse@ustc.edu.cn (G.Q. Zhang)

E-mail address: wuli8@163.com (J.H. Zhang)

‡ These authors contribute equally.

Experimental

In our experimentation, all of chemical reagents was purchased from Aladdin Industrial Corporation without any further purification.

Sample preparation

On the one hand, 0.5 g of melamine was dissolved in 20 mL DMSO (dimethylsulfoxide) to get solution A. On the other hand, 0.5 g cyanuric acid with different amounts of PVP were dissolved in 10 mL DMSO to get solution B. After complete dissolution with sonication, both solutions were mixed together and kept vigorous stirring for 10 min to get white precipitates. Subsequently, the products were centrifuged and washed three times by absolute ethanol before dried. Finally, the powder was calcined at 550 ^{o}C for 4 h under nitrogen atmosphere with a heating rate of 0.5 ^{o}C/min. The resultant materials were designated as CN, CNNC-0.05, CNNC-0.1 and CNNC-0.2 when the mass rate of PVP with the summation of melamine and cyanuric acid is 0, 0.05% (0.5 mg), 0.1% (1 mg) and 0.2% (2 mg), respectively.

The g-C_3N_4 porous spheres without plane distortion (CNNC-U) was prepared by calcinations the mixture of CN and 1 mg PVP at 550 ^{o}C for 4 h under nitrogen atmosphere with a heating rate of 0.5 ^{o}C/min.

Characterizations

The morphology were observed by scanning electron microscope (SEM, GeminiSEM 500, Germany) and transmission electron microscopy (TEM, Talox F200X, America). The thickness were confirmed by Atomic Force Microscope (AFM, MFP-3D Infinity, UK). The X-ray diffraction (XRD, TTR-III, Japan) pattern with a Cu Kα source was used to analyze crystalline structures. The chemical state of the as-prepared samples was performed with Fourier transform infrared spectroscopy (FTIR, Nicolet 8700, America), X-ray photoelectron spectroscopy (XPS, ESCA Lab 250,

UK) and Solid ^{13}C nuclear magnetic resonance (^{13}C NMR, Bruker AVANCE NEO 600 WB, Switzerland). The optical character of sample was obtained by UV-vis diffuse reflectance spectra (UV-vis DRS, SOLID3700, Japan). And the electron paramagnetic resonance (EPR) spectra was characterized by JES-FA200 (JEOL, Japan). The pore structures and surface areas were measured by the Brunauer-Emmett-Teller (BET) N_2 adsorption–desorption isotherms (TriStar II 3020, America).

Electrochemical measurements

Electrochemical measurements were tested by a CH Instruments 660E electrochemical workstation in a three electrode cell using Pt sheet, fluorine doped tin oxide (FTO) coated with catalysts and Ag/AgCl as the counter electrode, working electrode and reference electrode, respectively. 0.5 M Na_2SO_4 purified by Ar was used as the electrolyte.

The details of the preparation of working electrodes were described as follows: 10 mg catalyst was dispersed in 5 mL absolute ethanol including 10 uL nafion by sonication for about 30 min. Then, 10 μL of the suspension was drop-coated at FTO glass with an area of 1 × 1 cm^2. The FTO glasses were dried at 80 ^oC for 24 h to remove volatile organic compound before using. A 300 W xenon lamp (PLS-SXE 300, Beijing PerfectLight Co., Ltd. China) equipped with a cutoff filter to filter out the ultraviolet region below 420 nm ($\lambda > 420$ nm) was supplied as visible light source in photocurrent measurement at the -0.5 V bias potential vs. Ag/AgCl. Mott-Schottky plots were calculated by impedance-potential curve with the frequency of 1.0, 1.5 and 2.0 kHz, respectively. The electrochemical impedance spectrum (EIS) measurements were performed at a frequency range from 0.01 Hz to 100 kHz by applying AC voltage of 5 mV amplitude under open circuit potential conditions.

Photocatalytic Tests

The PHE experiments were accomplished by automatic online analysis system (Lasolar-6A, Beijing PerfectLight Co., Ltd. China) with 150 mL Pyrex reaction cell connecting to a water bath for maintaining the reactor temperature at 5 ^{o}C. The 10 mg sample was dispersed in 80 mL aqueous solution with 10 vol% triethanolamine (TEOA). And 1 wt% Pt (0.210 mL H_2PtCl_6, 1 g L^{-1}) was used as the co-catalyst by in-situ photo-deposition method. The air in the cell was evacuated by vacuum pump before irradiated. The light source is identical with photocurrent measurement. The generated hydrogen was analyzed by an on-line gas chromatography (GC 7900, Techcomp, China TCD, Ar carrier) connected with Lasolar-6A. The four cycles were performed. Similar with PHE, oxidation of benzyl alcohol and hydrogen evolution was carried out by replacing TEOA with benzyl alcohol. After finished, the resultant solution in the Pyrex reaction cell was obtained by removing photocatalyst. And the supernatant was extracted by 10 mL CH_2Cl_2 for three times and dried by anhydrous Na_2SO_4. The product was analyzed and quantified by gas chromatography (Agilent 7890B, FID, Ar carrier).

The quantum yield (QY) of CNNC-0.1 at different wavelength (420, 450 and 500 nm, $\lambda \pm 10$ nm) was measured by equation as following:

$$QY = \frac{the\ number\ of\ reacted\ electrons}{the\ number\ of\ incident\ photons} \times 100\%$$

$$= \frac{2 \times the\ number\ of\ evolved\ molecules}{the\ number\ of\ incident\ photons} \times 100\%$$

DFT calculation details

Our density functional theory (DFT) calculations are used Vienna *ab initio* simulation package (VASP)[1] with projected augmented wave (PAW) method[2]. The kinetic energy cutoff, which is the plane wave basis set, for the Kohn-Sham one-electron states is set to be 400 eV. The geometric optimizations and electronic

structure are calculated by using the Perdew-Burke-Ernzerhof (PBE) exchange-correlation potential within the generalized gradient approximation (GGA)[3]. Brillouin zone integration is used with a grid of 2 × 2 × 1 Monkhorst-Pack[4] k-mesh for geometry optimizations, and 4 × 4 × 1 k-mesh for the electronic structure calculations. For the size of all geometry structures are kept fixed but atomic positions are fully relaxed with the convergence criteria of energy and force set at 10^{-4} eV and 0.01 eV/Å, respectively. The vacuum thickness along the z axis is set to 20 Å, which is large enough to avoid interaction between periodic images. To study the adsorption of N doped graphene on the g-C_3N_4 involved in photocatalytic splitting of water, we have considered an N doped carbon-ring adsorbed to 3 × 3 × 1 supercell of the g-C_3N_4.

Figures

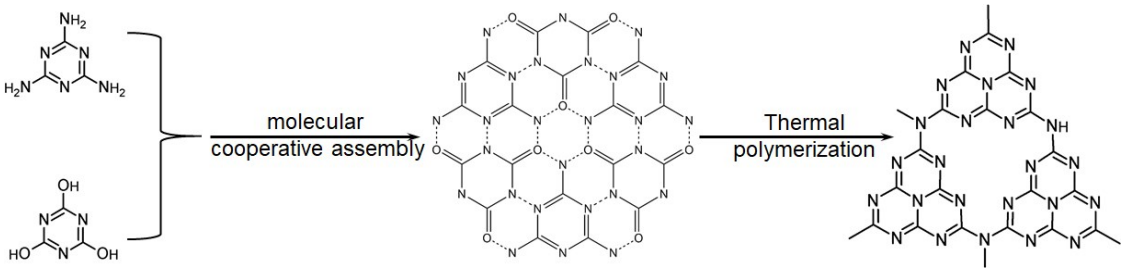

Fig. S1 The formation mechanism of g-C_3N_4 porous spheres.

Melamine and cyanuric acid are not easy to be dissolved in most solvents, yet both of them are soluble in dimethyl sulfoxide (DMSO). Therefore, both compounds were first dissolved in DMSO, respectively. Then, hydrogen-bonded supramolecular aggregates by molecular cooperative assembly have been formed when the equimolar ratio of melamine and cyanuric acid were mixed together.[5]

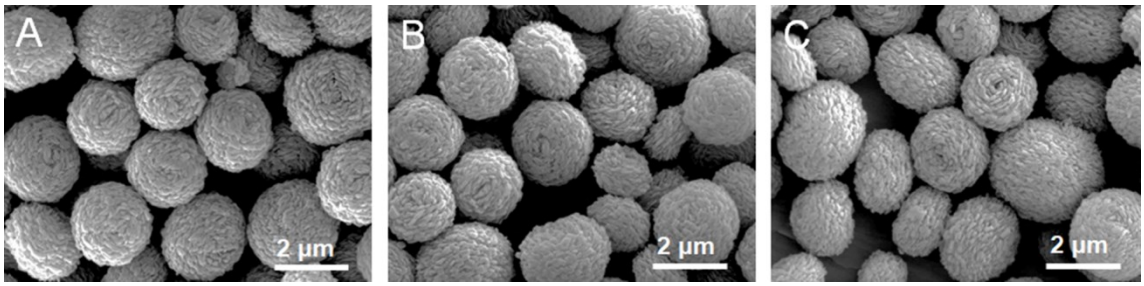

Fig. S2 SEM image of melamine - cyanuric acid supramolecular spheres with (A) 0 mg, (B) 0.5 mg and (C) 2 mg PVP.

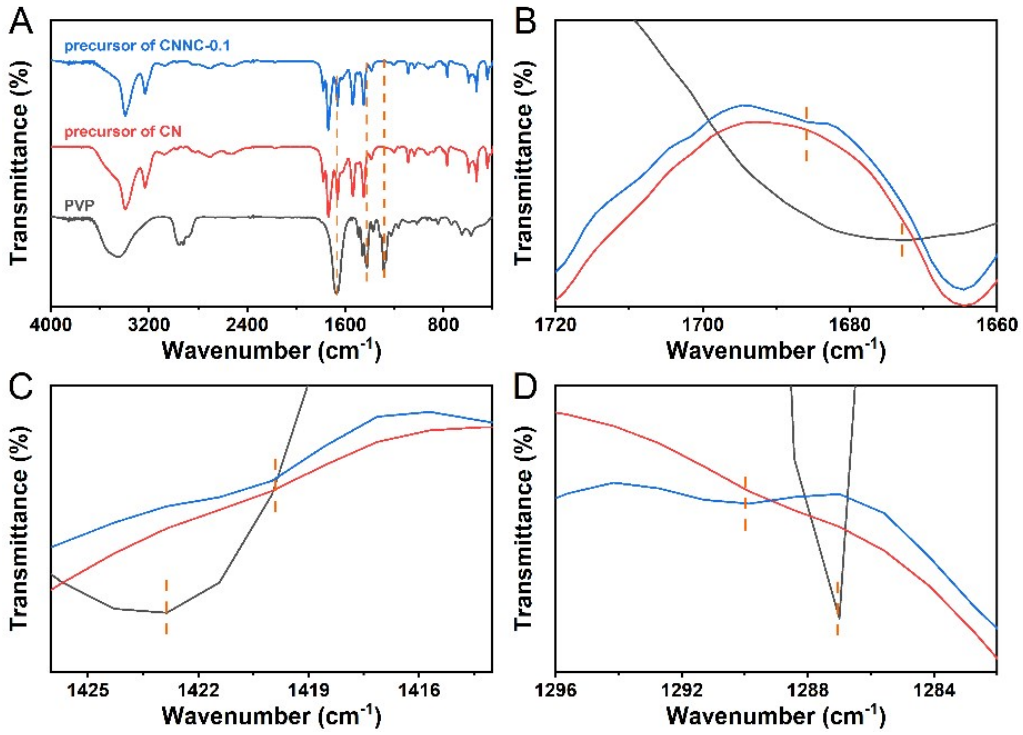

Fig. S3 FTIR spectra of PVP, precursor of CN and precursor of CNNC-0.1.

The morphology of supramolecular spheres precursor with and without PVP do not show significant difference (Fig. 1B and Fig. S2, ESI†), and solid spheres structure can be observed by TEM (Fig. 1B inside). The porous structure can be observed due to the volatilization of ammonia during thermal polymerization (Fig. 1C, D and Fig. S4, ESI†). However, a more complete spherical morphology can be preserved when PVP is added into precursor (Fig. S4), which may be due to the interaction between PVP and the precursor. To prove our hypothesis, the PVP, precursor of CN and precursor of CNNC-0.1 were investigated by FTIR spectra. The typical IR peaks of PVP at 1672, 1423 and 1287 cm^{-1} are ascribed to stretching vibration of carbonyl group ν(C=O), bending vibration of δ(CH_2) and stretching vibration of ν(C-N), respectively.[6] When PVP was introduced into precursor, a weak IR peak appeared and exhibited sort of shift, indicating the interaction was established between PVP and the

precursor. The PVP molecules in the supermolecules may be like agglomerant, which guarantee a completer spherical morphology. Therefore, the specific surface area of CNNC is drastically reduced.

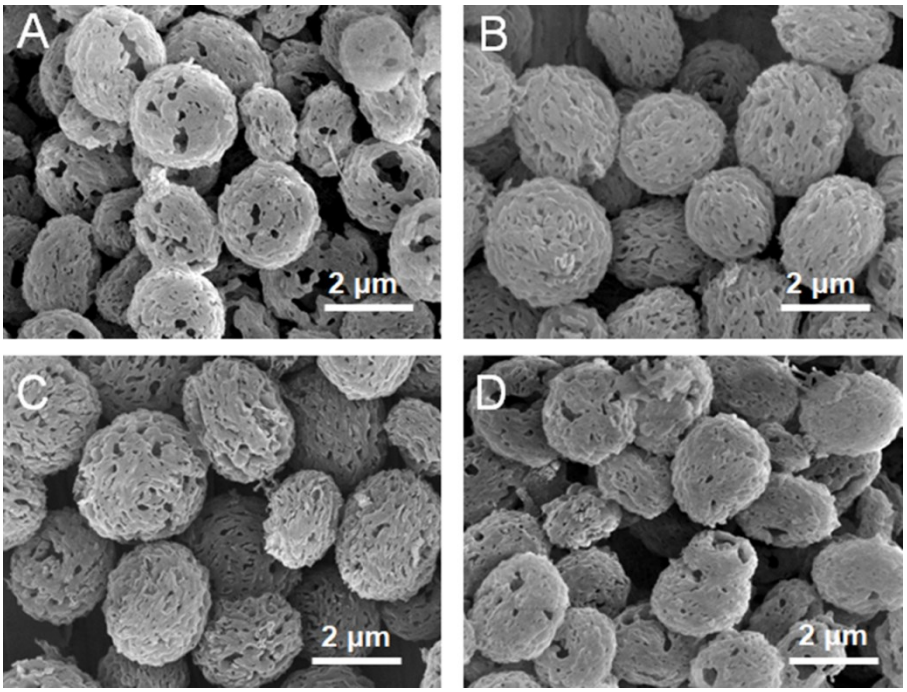

Fig. S4 SEM image of (A) CN, (B) CNNC-0.05 (C) CNNC-0.2 and (D) CNNC-U.

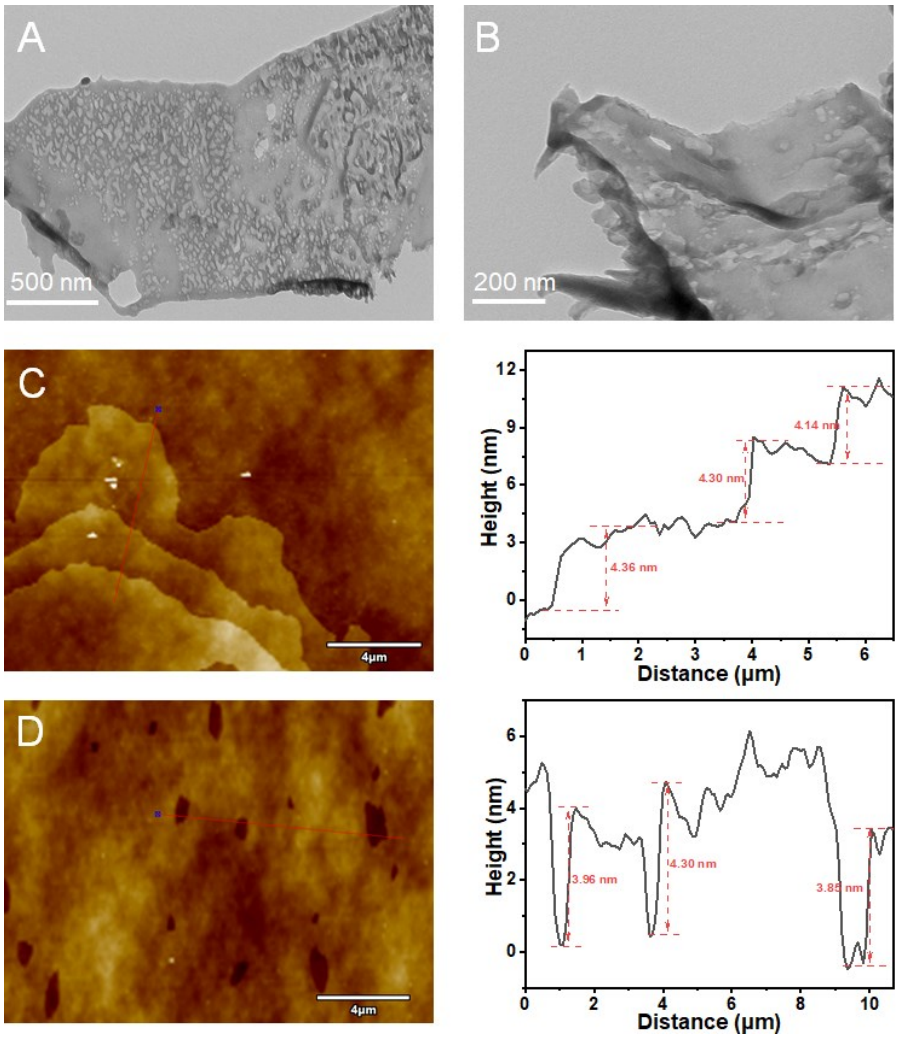

Fig. S5 The TEM (A, B) and AFM (C, D) images of the ultrathin porous nanosheets. The result indicates that the porous spheres are assembled by ultrathin porous nanosheets with thickness approximately 4.3 nm.

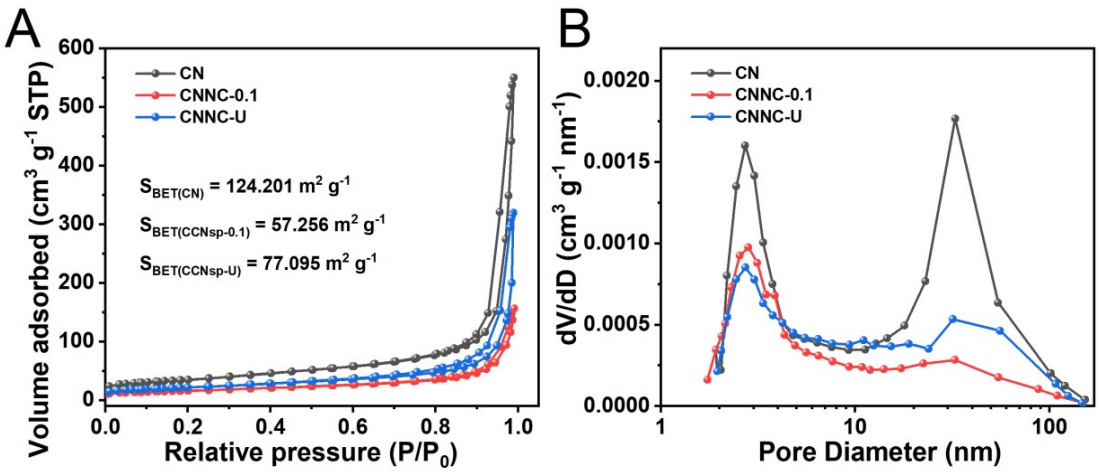

Fig. S6 (A) N_2 adsorption–desorption isotherms of CN, CNNC-0.1 and CNNC-U porous spheres, respectively and (B) the corresponding pore size distribution curve.

A typical type-IV curves and a broad pore size distribution in mesoporous range of all samples can be observed by BET N_2 adsorption–desorption isotherms, suggesting well-defined mesoporous structures.

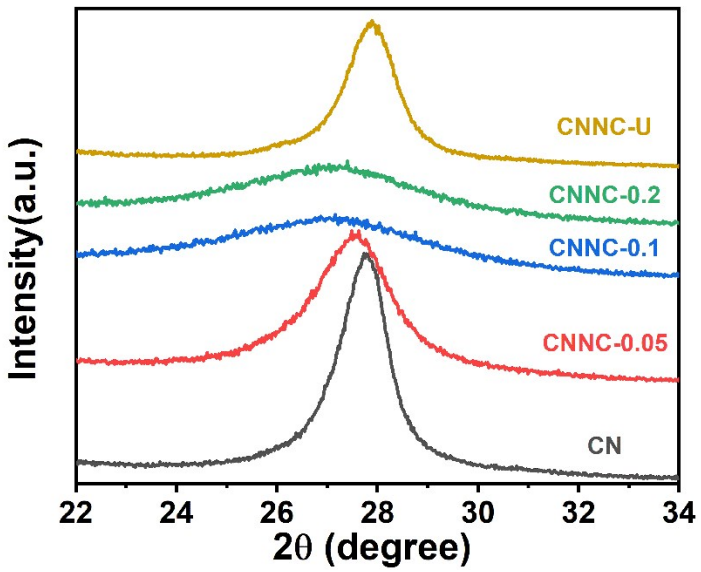

Fig. S7 The XRD patterns of as-prepared different samples in the range from 22° to 34°.

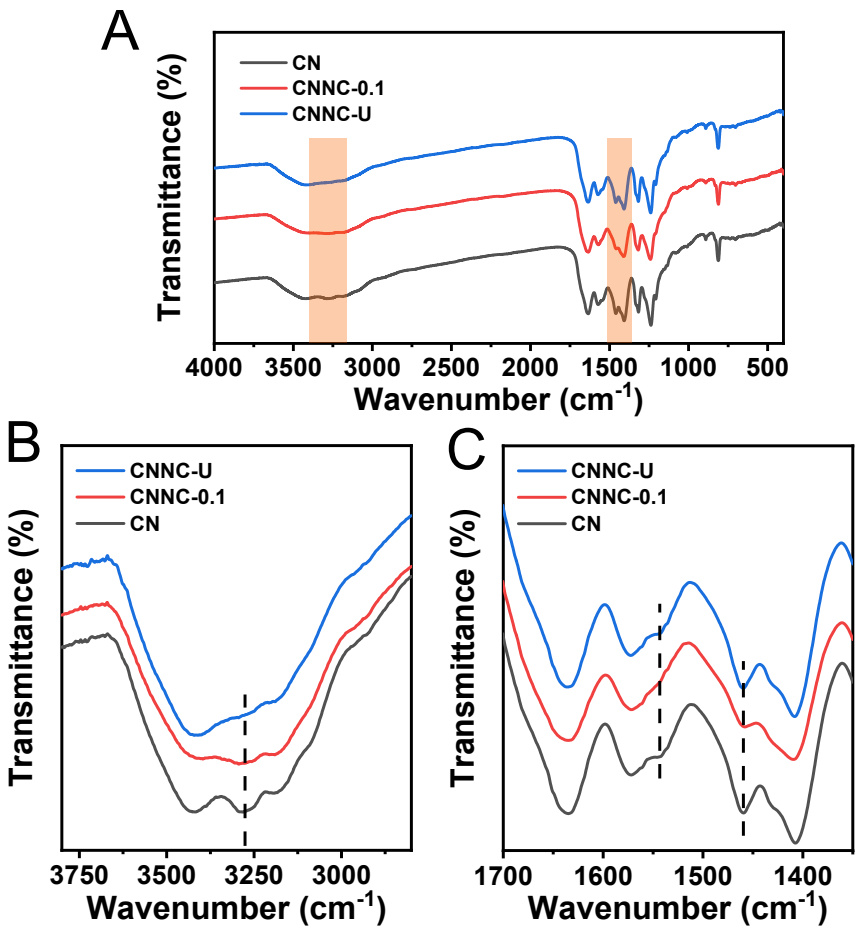

Fig. S8 FTIR spectra of CN, CNNC-0.1 and CNNC-U porous spheres.

A broad peaks between 3000 and 3500 cm^{-1} of FTIR spectrum for CN, CNNC-0.1 and CNNC-U porous spheres are assigned to the N-H group stretching vibrations peaks.[7] Specifically, the indistinct N-H group stretching peaks of CNNC-0.1 and CNNC-U in the intensity manifests that N-H group was took away at the time of annealing when PVP was imported to porous spheres precursor. What's more, the disappeared speaks of C-N heterocycles stretching vibration modes at 1458 cm^{-1} and 1542 cm^{-1} were happened just at CNNC-0.1 sample, indicating that the in-plane repeating units has been broken tremendously just when calcining precursor containing of PVP.[7] This consequence is compatible with weakened peaks intensities of XRD spectra (Fig. 1E) and will be further verified by XPS as follows.

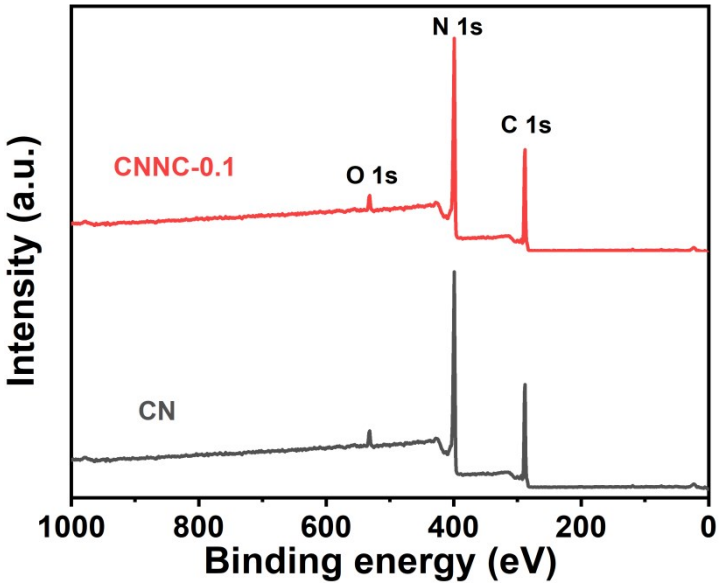

Fig. S9 The survey spectra of the as-prepared CN and CNNC-0.1 porous spheres.

The CN and CNNC-0.1 samples were identified further by XPS. The survey spectra reveal that the surface of the CN and CNNC-0.1 samples contains C, N and O elements. The residual oxygen could originate from the adsorbed oxygen or water vapor in air.[7a, 8]

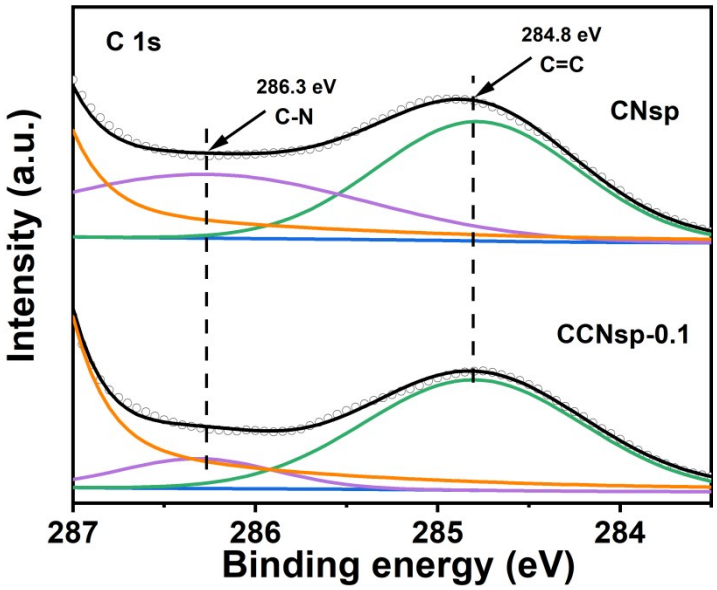

Fig. S10 High-resolution XPS spectra of C 1s in the range from 283.5 to 287 eV.

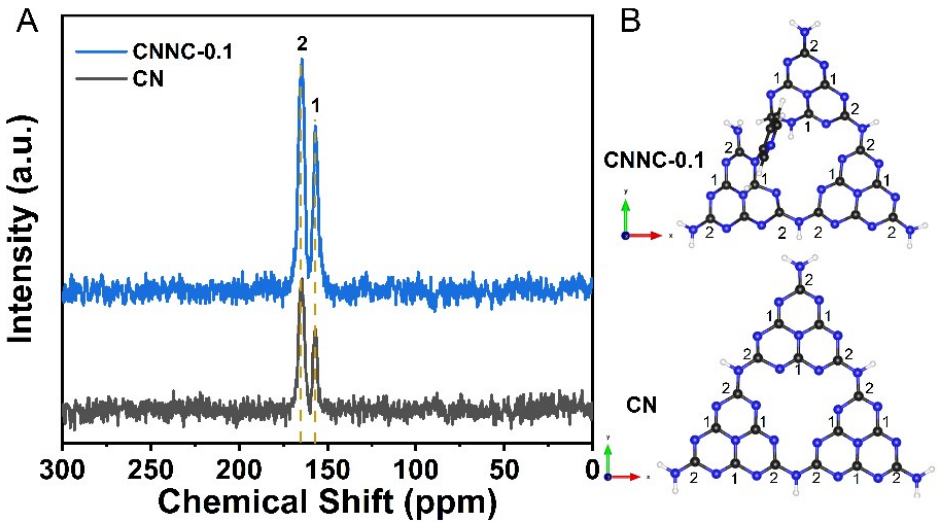

Fig. S11 (A) Solid ^{13}C NMR spectra for CN and CNNC-0.1 and (B) a plausible structure of CN and CNNC.

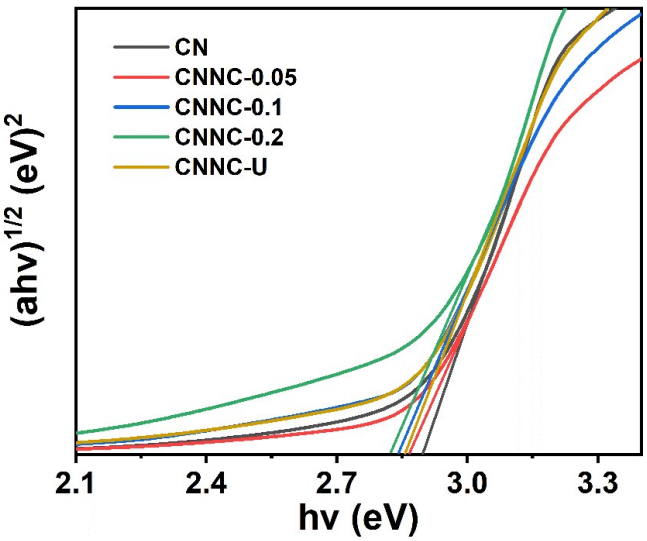

Fig. S12 Tauc plot of the as-prepared different samples.

The band gap of the CN is estimated to be 2.91 eV. The slightly increased bandgap could be accredited to the quantum confinement effect since the thickness of the nanosheet subunit for the porous spheres is only about 4.3 nm determined by the AFM measurement. (Fig. S5). Compared to the CN, the decrease of the band gap for the others (2.86 eV of CNNC-0.05, 2.84 eV of CNNC-0.1 and 2.81 eV of CNNC-0.2) could be ascribed to the import of N doped carbon resulting from the carbonization of PVP. The narrower bandgap and extended absorption in visible-light range improve the utilization for low energy light of the major component of sun light on the earth.

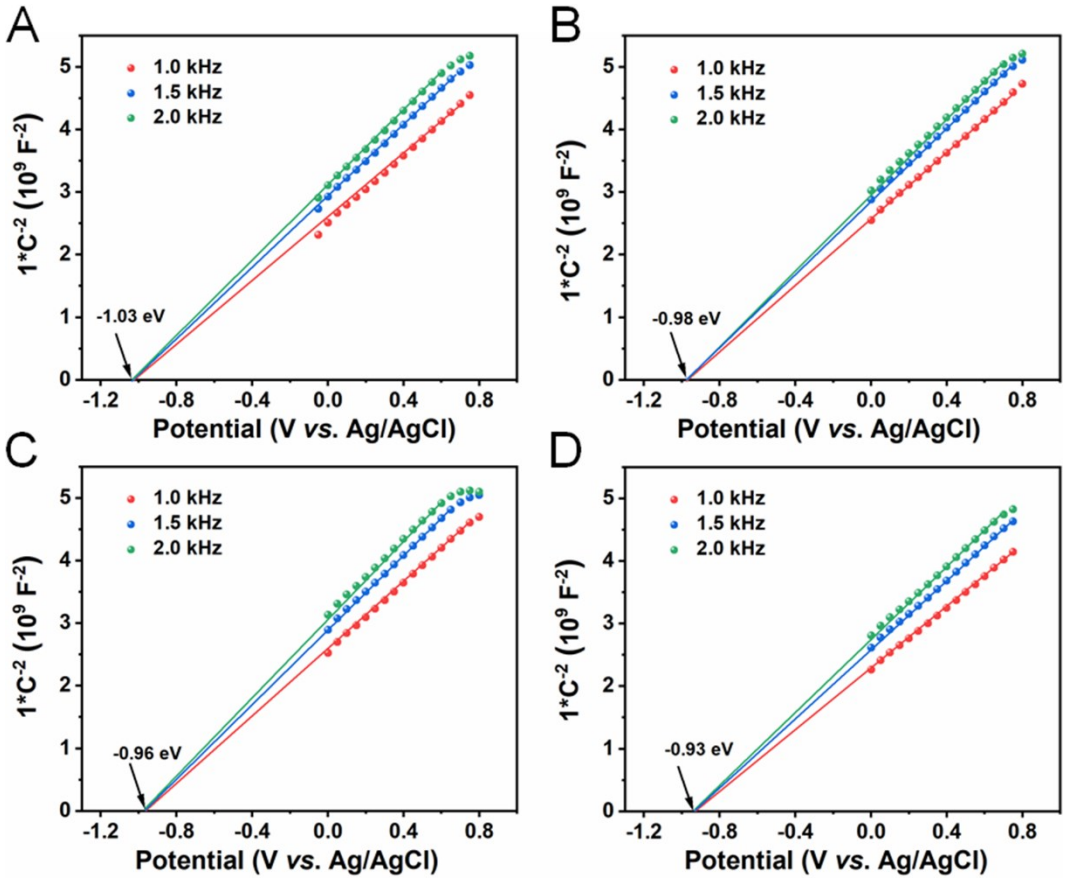

Fig. S13 Mott−Schottky plots of the as-prepared (A) CN, (B) CNNC-0.05 porous spheres, (C) CNNC-0.1 porous spheres and (D) CNNC-0.2 porous spheres.

Generally, the flat-band potentials (V_{fb}) of the samples were measured using Mott-Schottky plots. The positive slope of the Mott-Schottky plots for photocatalyst semiconductor materials samples indicated the n-type nature.[9] And the V_{fb} is located just below the bottom of conduction band (CB) for an n-type semiconductor.[10] This method is widely used to estimate the position of CB for n-type semiconductor materials.[11] Therefore, the conduction band position of the as-prepared CN, CNNC-0.05, CNNC-0.1 and CNNC-0.2 porous spheres could be estimated to -1.03, -0.98, -0.96 and -0.93 V vs. Ag/AgCl electrode, pH = 7, respectively.

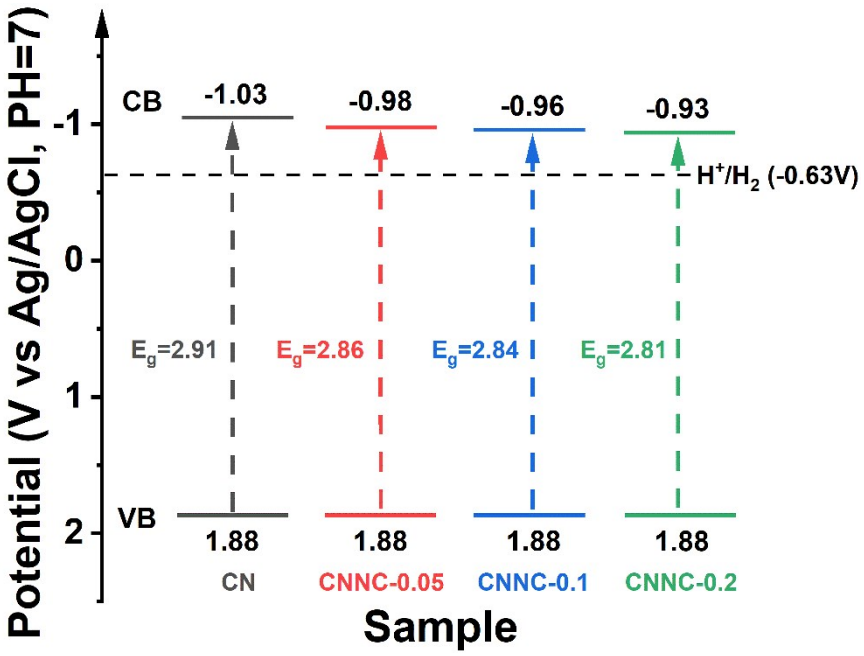

Fig. S14 Electronic band structures of as-prepared samples with different content of PVP.

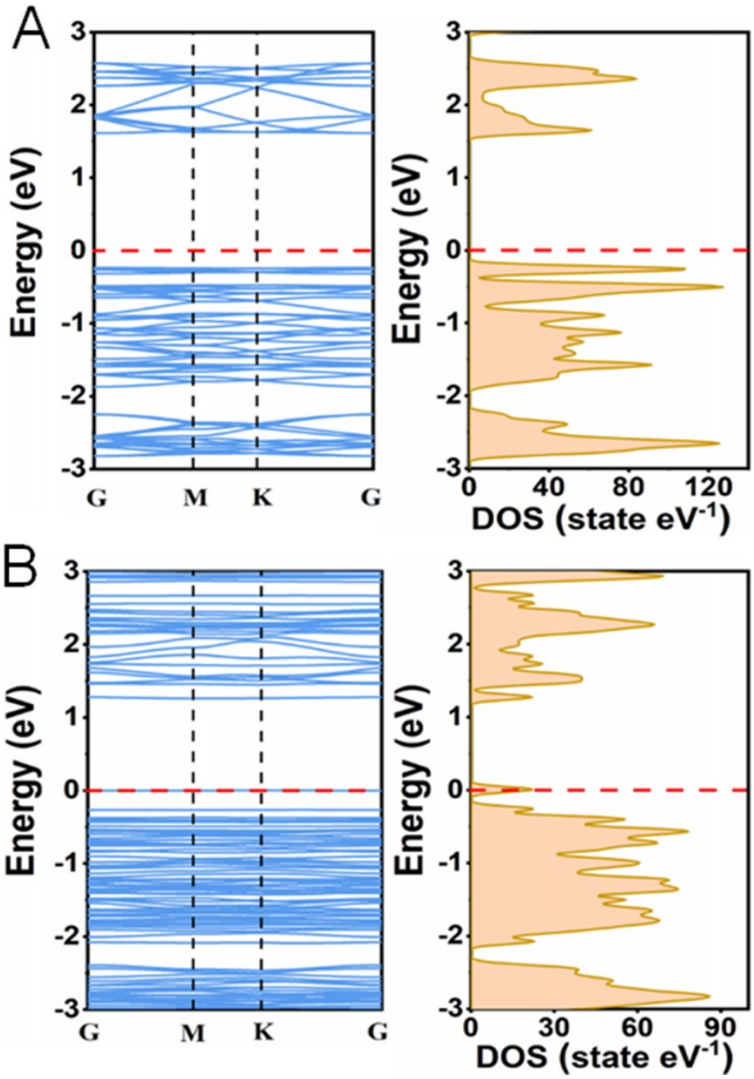

Fig. S15 Calculated band structures and density of state (DOS) of (A) CNsp and (B) CNNC porous spheres.

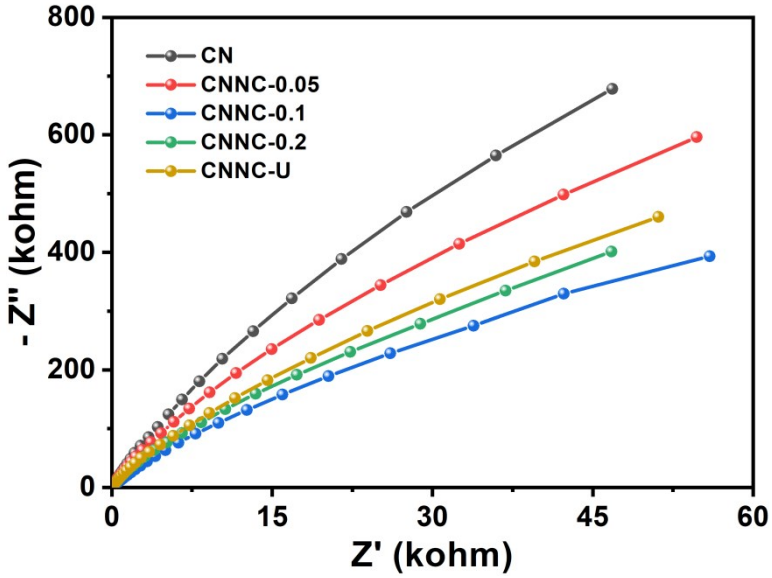

Fig. S16 EIS data of the corresponding samples.

The EIS shows that the arc radius of Nyquist plots for CNNC-0.1 porous spheres samples were smallest than that of others, which confirmed that the CNNC-0.1 porous spheres possess lowest interfacial charge-transfer resistance and an effective separation of the photogenerated e^-–h^+ pairs than CN, thereby allowing faster charge transfer.

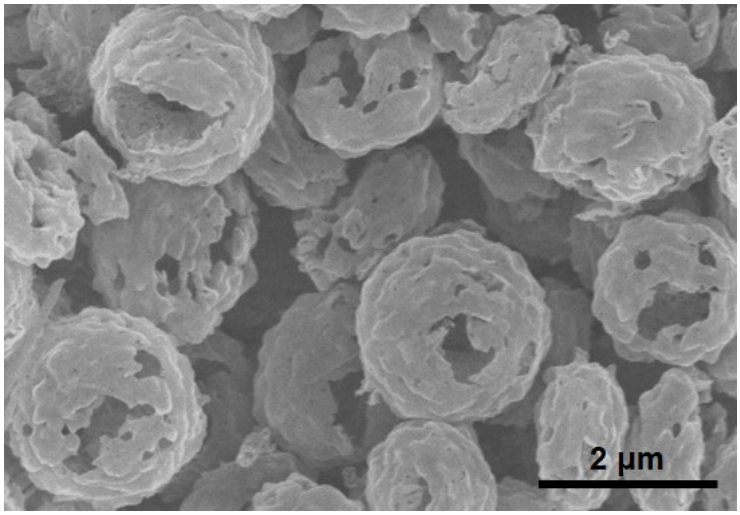

Fig. S17 SEM images of CNNC-0.1 porous spheres after photocatalytic test.

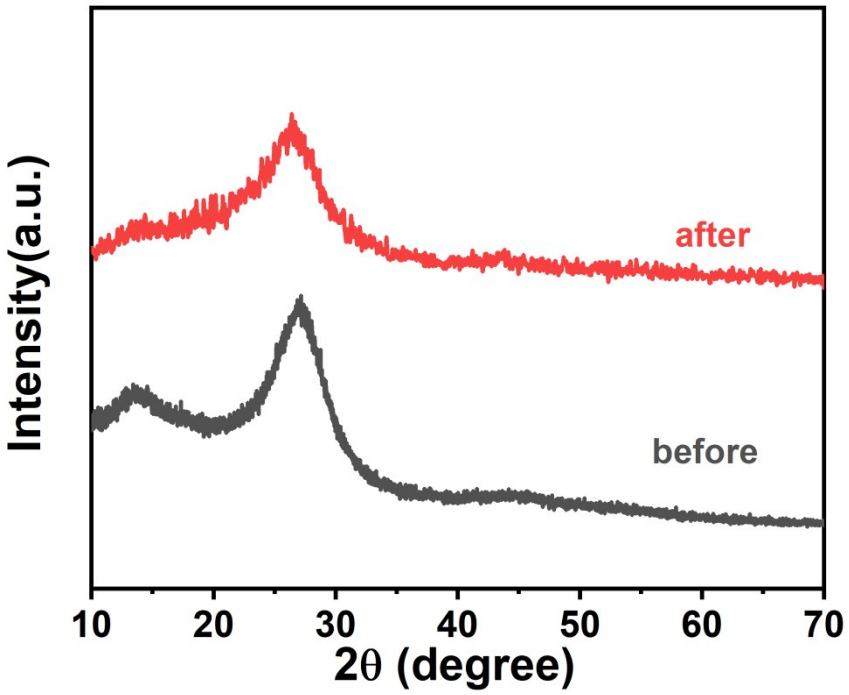

Fig. S18 XRD patterns different of the CNNC-0.1 porous spheres samples before and after photocatalytic test.

The morphologies and crystal structure of CNNC-0.1 exhibit no change obviously, indicating the good photostability and durability.

Table S1 Atomic ratio of CN and CNNC-0.1 from XPS data.

Samples	Atomic ratio		
	C	**N**	**C/N**
CN	42.49%	57.51%	0.74
CNNC-0.1	42.71%	57.29%	0.75

Table S2 Relative ratios of N-C=N, C-N and C-C determined by C1s XPS spectra.

Samples	**N-C=N**	**C-N**	**C-C**
CN	91.86%	3.72%	4.42%
CNNC-0.1	94.72%	0.85%	4.43%

Table S3 Relative ratios of N-C=N, N-$(C)_3$, C-NH_3 and π-excitation determined by N1s XPS spectra.

Samples	**N-C=N**	**N-$(C)_3$**	**C-NH_3**	**π-excitation**
CN	62.45%	24.98%	6.93%	5.64%
CNNC-0.1	70.08%	18.59%	6.49%	4.84%

Table S4 Summary of the photocatalytic hydrogen evolution performance of g-C_3N_4 based catalysts.

Catalyst	Cocatalyst	Sacrificial	Light source	H_2 rate (mmol h^{-1} g^{-1})	Ref.
CNNC-0.1	Pt, 1 wt %	10 vol % TEOA	300 W Xe lamp (λ>420 nm)	7.86	**This work**
CQD/g-C_3N_4	Pt, 3 wt %	25 vol % Methanol	300 W Xe lamp (λ>400 nm)	3.54	[12]
N-doped g-C_3N_4	Pt, 3 wt %	10 vol % TEOA	300 W Xe lamp (λ>420 nm)	1.28	[13]
CCN	Pt, 3 wt %	10 vol % TEOA	300 W Xe lamp (λ>420 nm)	0.53	[14]
Pt-CN	--	10 vol % TEOA	300 W Xe lamp	6.36	[15]
C-PDA–g-C_3N_4	Pt, 1.5 wt %	10 vol % TEOA	300 W Xe lamp (λ>400 nm)	0.81	[16]
CQDs/C_3N_4	Pt, 3 wt %	Bisphenol A	300 W Xe lamp (λ>420 nm)	0.15	[17]
N-GQDs/CN-U	Pt, 1 wt %	10 vol % TEOA	300 W Xe lamp (λ>420 nm)	2.18	[18]
Ag/CQDs/g-C_3N_4	--	10 vol % TEOA	300 W Xe lamp (λ>550 nm)	0.63	[19]
PCN-U	Pt, 3 wt %	10 vol % TEOA	300 W Xe lamp (λ>400 nm)	5.22	[20]
CNS-Pt	Pt, 1 wt %	10 vol % TEOA	350 W Xe lamp (λ>420 nm)	4.21	[21]
O-g-C_3N_4	Pt, 3 wt %	10 vol % TEOA	300 W Xe lamp (λ>420 nm)	8.87	[22]
P-DCN	Pt, 3 wt %	10 vol % TEOA	300 W Xe lamp (λ>420 nm)	2.09	[23]
P-g-C_3N_4	Pt, 1 wt%	20 vol% TEOA	300W Xe lamp (λ ⩾ 400 nm)	1.60	[24]

Table S5 Comparison of H_2 production coupled with benzyl alcohol oxidation over various photocatatlysts reported in literatures.

Photocatatlyst	Reaction medium	Light source	H_2 rate (μmol h^{-1} g^{-1})	Benzaldehyde rate (μmol h^{-1} g^{-1})	Ref.
CNNC-0.1[a]	Water	300 W Xe lamp (λ ⩾ 420 nm)	464.75	463.75	This work
SCN-HMS[a]	Water	300 W Xe lamp (λ ⩾ 420 nm)	376	387	5b
$^{NCN}CN_x$-NiP[b]	Water (pH=4.5)	300 W Xe lamp (λ ≥ 400 nm)	178.92	165	25
RuCat/Pt-g-C_3N_4[b]	Water	300 W Xe lamp (λ ≥ 400 nm)	255	152.44	26
ZnS-Ni_xS_y[b]	Water	500 W Xe lamp	3648	3301	27
$Zn_3In_2S_6$-W[c]	Water	300 W Xe lamp (λ ≥ 380 nm)	1772	1830	28
Pt–TiO_2[d]	CH_3CN	3 × 3 W LED (λ = 366 nm)	960	902.4	29

[a]reaction temperature: 5 °C; [b]reaction temperature: 25 °C; [c]reaction temperature: 10 °C; [d]reaction temperature: 40 °C

References:

1. (a)G. Kresse and J. Hafner, *Phys. Rev. B*, 1993, **47**, 558-561;(b)G. Kresse and J. Furthmüller, *Phys. Rev. B*, 1996, **54**, 11169-11186.
2. G. Kresse and D. Joubert, *Phys. Rev. B*, 1999, **59**, 1758-1775.
3. J. P. Perdew, K. Burke and M. Ernzerhof, *Phys Rev Lett*, 1996, **77**, 3865-3868.
4. H. J. Monkhorst and J. D. Pack, *Phys. Rev. B*, 1976, **13**, 5188-5192.
5. (a)Y. S. Jun, E. Z. Lee, X. C. Wang, W. H. Hong, G. D. Stucky and A. Thomas, *Adv. Funct. Mater.*, 2013, **23**, 3661-3667;(b)F. Zhang, J. Li, H. Wang, Y. Li, Y. Liu, Q. Qian, X. Jin, X. Wang, J. Zhang and G. Zhang, *Appl. Catal. B*, 2020, **269**, 118772.
6. (a)T. Zhu, S. Chang, Y.-F. Song, M. Lahoubi and W. Wang, *Chem. Eng. J.*, 2019, **373**, 755-766;(b)C. Wu, S. Wang, J. Zhao, Y. Liu, Y. Zheng, Y. Luo, C. Ye, M. Huang and H. Chen, *Adv. Funct. Mater.*, 2019, **29**, 1901722.
7. (a)H. Yu, R. Shi, Y. Zhao, T. Bian, Y. Zhao, C. Zhou, G. I. N. Waterhouse, L. Z. Wu, C. H. Tung and T. Zhang, *Adv. Mater.*, 2017, **29**, 1605148;(b)P. Niu, L. L. Zhang, G. Liu and H. M. Cheng, *Adv. Funct. Mater.*, 2012, **22**, 4763-4770.
8. F. Dong, Z. W. Zhao, T. Xiong, Z. L. Ni, W. D. Zhang, Y. J. Sun and W. K. Ho, *ACS Appl. Mater. Interfaces*, 2013, **5**, 11392-11401.

9. J. Boltersdorf, I. Sullivan, T. L. Shelton, Z. K. Wu, M. Gray, B. Zoellner, F. E. Osterloh and P. A. Maggard, *Chem. Mater.*, 2016, **28**, 8876-8889.
10. (a)S. J. Hong, S. Lee, J. S. Jang and J. S. Lee, *Energy Environ. Sci.*, 2011, **4**, 1781-1787;(b)X.-H. Li and M. Antonietti, *Chem. Soc. Rev.*, 2013, **42**, 6593-6604.
11. (a)J. P. Zou, D. D. Wu, J. M. Luo, Q. J. Xing, X. B. Luo, W. H. Dong, S. L. Luo, H. M. Du and S. L. Suib, *ACS Catal.*, 2016, **6**, 6861-6867;(b)Z. Tong, D. Yang, Z. Li, Y. Nan, F. Ding, Y. Shen and Z. Jiang, *ACS Nano*, 2017, **11**, 1103-1112;(c)S. Feng, T. Wang, B. Liu, C. Hu, L. Li, Z. J. Zhao and J. Gong, *Angew. Chem. Int. Ed.*, 2020, **59**, 2044-2048;(d)Y. X. Pan, Y. You, S. Xin, Y. Li, G. Fu, Z. Cui, Y. L. Men, F. F. Cao, S. H. Yu and J. B. Goodenough, *J. Am. Chem. Soc.*, 2017, **139**, 4123-4129;(e)S. Sun, M. Watanabe, J. Wu, Q. An and T. Ishihara, *J. Am. Chem. Soc.*, 2018, **140**, 6474-6482.
12. Y. Wang, X. Liu, J. Liu, B. Han, X. Hu, F. Yang, Z. Xu, Y. Li, S. Jia, Z. Li and Y. Zhao, *Angew. Chem. Int. Ed.*, 2018, **57**, 5765-5771.
13. Y. Zhou, L. Zhang, W. Huang, Q. Kong, X. Fan, M. Wang and J. Shi, *Carbon*, 2016, **99**, 111-117.
14. H. Li, F. Li, Z. Wang, Y. Jiao, Y. Liu, P. Wang, X. Zhang, X. Qin, Y. Dai and B. Huang, *Appl. Catal. B Environ.*, 2018, **229**, 114-120.
15. X. Li, W. Bi, L. Zhang, S. Tao, W. Chu, Q. Zhang, Y. Luo, C. Wu and Y. Xie, *Adv. Mater.*, 2016, **28**, 2427-2431.
16. F. He, G. Chen, Y. Yu, Y. Zhou, Y. Zheng and S. Hao, *Chem. Commun.*, 2015, **51**, 6824-6827.
17. G. Zhang, Q. Ji, Z. Wu, G. Wang, H. Liu, J. Qu and J. Li, *Adv. Funct. Mater.*, 2018, **28**, 1706462.
18. J.-P. Zou, L.-C. Wang, J. Luo, Y.-C. Nie, Q.-J. Xing, X.-B. Luo, H.-M. Du, S.-L. Luo and S. L. Suib, *Appl. Catal. B Environ.*, 2016, **193**, 103-109.
19. J. Qin and H. Zeng, *Appl. Catal. B Environ.*, 2017, **209**, 161-173.
20. P. Yang, H. Ou, Y. Fang and X. Wang, *Angew. Chem. Int. Ed.*, 2017, **56**, 3992-3996.
21. M. Liu, P. Xia, L. Zhang, B. Cheng and J. Yu, *ACS Sustain. Chem. Eng.*, 2018, **6**, 10472-10480.
22. X. She, J. Wu, J. Zhong, H. Xu, Y. Yang, R. Vajtai, J. Lou, Y. Liu, D. Du, H. Li and P. M. Ajayan, *Nano Energy*, 2016, **27**, 138-146.
23. D. Zhang, Y. Guo and Z. Zhao, *Appl. Catal. B Environ.*, 2018, **226**, 1-9.
24. J. Ran, T. Y. Ma, G. Gao, X.-W. Du and S. Z. Qiao, *Energy Environ. Sci.*, 2015, **8**, 3708-3717.
25. H. Kasap, C. A. Caputo, B. C. M. Martindale, R. Godin, V. W.-h. Lau, B. V. Lotsch, J. R. Durrant and E. Reisner, *J. Am. Chem. Soc.*, 2016, **138**, 9183-9192.
26. F. Li, Y. Wang, J. Du, Y. Zhu, C. Xu and L. Sun, *Appl. Catal. B Environ.*, 2018, **225**, 258-263.
27. H. Hao, L. Zhang, W. Wang, S. Qiao and X. Liu, *ACS Sustainable Chem. Eng.*, 2019, **7**, 10501-10508.
28. X. Ye, Y. Chen, Y. Wu, X. Zhang, X. Wang and S. Chen, *Appl. Catal. B*, 2019, **242**, 302-311.

29. K. Imamura, H. Tsukahara, K. Hamamichi, N. Seto, K. Hashimoto and H. Kominami, *Appl. Catal. A*, 2013, **450**, 28-33.